Adaptive Passivity Compensation of Grid-following MMC for Stable Grid Integration

Pengxiang Huang, *Student Member, IEEE*, and Luigi Vanfretti, *Senior Member, IEEE*

***Abstract*—Grid following-modular multilevel converter (GFL-MMC) are founded to form high-frequency resonance (HFR) with ac grid across a wide frequency range, in which the delay-induced passivity shortage of MMC is identified as the root-cause. This paper presents an adaptive damping control method based on online resonance detection, which can detect multiple HFRs online and mitigate them selectively via multiple-complex coefficient-filter (MCCF) based narrowband damping control. An extended application of iterative-interpolated discrete Fourier transform (i-IpDFT) is proposed to accurately detect the HFRs from the MMC current. The adaptive programming and conducting of multi-tuned damping control are also explained. In addition, this paper presents an algorithm for identifying early detected HFRs that disappear due to grid variation, and readjusting multi-tuned damping control to account for the change. Hence, the proposed method is robust against varing grid conditions. The EMT simulation results are presented and demonstrate the performance of the proposed method.**

***Index Terms*—Grid-following MMC, passivity, narrowband damping, resonance detection, adaptive control.**

I. Introduction

A. Motivation

HIGH frequency resonance (HFR) between MMC and ac grid is formed during grid integration when the resonance frequency falls into the non-passive (i.e., negative damping) region of MMC, unless grid resistance can sufficiently make net-damping positive [1]. As it is known, non-passive region of MMC in high-frequency range (i.e., few hundred Hz to Nyquist frequency) is caused by time delay, and it appears periodically over a wide frequency range, resulting in multiple resonances simultaneously [2]. Compensating passivity in such a wide frequency range is challenging, since the effectiveness of active damping is drastically reduced by the same time delay. The multi-tuned narrowband damping with phase-lead unit is thus preferred as it can add virtual positive damping to MMC at multiple pre-selected ranges, and it can also compensate the delay-generated phase shift on each designed damping functions [2]. However, HFR varies with the change of MMC control modes, system operating condition and ac grid configuration. Therefore, it cannot be predicted offline and tackled by incorporating the damping control in advance. This has raised concerns about detecting potential or existing HFRs in real time and making use of the adaptive damping control to avoid or suppress it.

B. Literature Review

Adaptive narrowband damping requires an estimation of resonance frequency with both high accuracy and low report latency due to two facts as: 1) Inaccurate estimation makes adopted narrowband damper center to neighboring frequencies of resonance, which may shift the resonance frequency outside the pre-defined damping band and leads to unintended effects; 2) If it is not suppressed quickly, the high-frequency oscillation component could trip relay in a few tens of milliseconds or even quicker.

Resonance frequency can be determined by measuring grid impedance via the current perturbation from GFL-MMC into the grid, and by evaluating impedance ratio of grid against MMC to determine resonance frequency, which is so-called online impedance measurement-based method [3]. Doing so are usually plagued by problems of: 1) significant conflict between detection accuracy and speed requirement; 2) low immunity to noise and background harmonics; 3) detection accuracy is sensitive to perturbation signal design; 4) controller and modulator further decreases the perturbation performance.

A more straightforward approach to estimate resonance frequency is based on analysis of the oscillating component of MMC current when resonance has occurred, which is so-called online resonance detection. The discrete Fourier transform (DFT) is generally used to measure the frequency of oscillating components in such approach. To attain low reporting latency and minimize incoherent sampling effects, windowed three-point interpolated DFT (IpDFT) is well-studied in [4], [5]. Nevertheless, IpDFT does not account for spectral interference generated by harmonic or inter-harmonic components in the vicinity of estimated frequency. To provide precise estimation in the presence of spectral interference, [6] proposed an iterative IpDFT (i-IpDFT) that iteratively eliminates the spectral interference from nearby inter-harmonic components. However, the i-IpDFT is proposed for the estimation of the fundamental frequency in PMU application, and its use to detect resonance frequencies requires further discussion.

After the resonance is detected, its frequency and magnitude are provided as the guideline for adaptive damping design. In [7], a single-tuned band-pass filter based damping control is programmed to detected resonance frequency, which adds virtual damping to inverter and suppresses the inverter-grid resonance. However, [7] does not consider the time delay effect on damping function nor lacks the capability of mitigating multiple resonances. To suppress multiple HFRs, adaptive notch filters (ANFs) are used to disable the time delay effect around multiple resonance frequencies detected by IpDFT [8]. However, [8] assumes the multiple HFRs appear consecutively, in other words, HFR occurs at only one frequency at a time. Under this assumption, the frequency estimation error caused by spectral interference is negligible. Additionally, since ANFs based damping control lacks the capability of

providing additional amount of positive damping to MMC-grid system, there will either be an under damped resonance with relatively long decaying time or turn an unstable resonance into a critically damped resonance depending on the grid resistance.

In this work, multiple resonance frequencies are first identified based on i-IpDFT analysis of MMC current and proposed resonance identification algorithm, the detected frequencies are then used to design a multi-tuned narrowband damping controller based on voltage feed-forward. In doing so, the MMC passivity is concurrently compensated in multiple frequency ranges and multiple HFRs are thus suppressed. We are specifically interested in how to precisely detect multiple existing HFRs, how to adaptively program and conduct multi-tuned narrowband damping control, and how to adjust damping control under varying grid conditions. With this aim, the algorithm for detecting multiple HFRs and the algorithm for designing and updating adaptive damping control are proposed.

C. Contributions

The specific contributions of this paper are the following:

- Proposing the extended application of i-IpDFT with compensation for spectral interference to accurately estimate the frequency of spectral-peaks in short-time spectrum analysis.
- Proposing an algorithm to identify electrical transient signal and resonance oscillation signals.
- Proposing a strategy to adaptively design and conduct the multi-tuned narrowband damping control for the mitigation of multiple HFRs
- Proposing an adaption algorithm to reconfigure all the employed active damping controls, removing the ones that are redundant after changed grid conditions.

D. Organization

The rest of the paper is organized as follows. Section II describes the system under study and discusses the passivity-based stability analysis. Section III presents the design and implementation of multi-tuned narrowband damping control. Section IV demonstrates how to adaptively employ and coordinate multiple damping functions based on the HFRs identified by the proposed detection and identification algorithm. Furthermore, an adaption rule is proposed to automate the process of disconnecting the unnecessary employed damping control after grid variation. The simulation demonstrations of the proposed adaptive passivity compensation method are presented in section V, the results show the method provides an automatic and effective way to mitigate multiple HFRs and is robust under varying grid conditions. Section VI concludes the work.

II. System and Voltage-based Damping Control

A. System and Passivity-Based Stability Analysis

Fig. 1 illustrates the single-line diagram of the GFL-MMC connected to the grid through step-up transformer and long

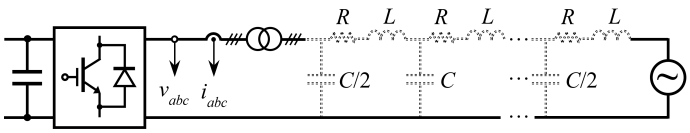

Fig. 1. Schematic of GFL-MMC connected to the grid via ac transmission.

overhead lines or HVAC onshore cable system. Since both long overhead line and cable can be modeled as an equivalent π-section line, this work is conducted only on GFL-MMC against long overhead lines and grid, while the number of π-sections is selected to guarantee the modeling accuracy to the Nyquist frequency $f_s/2$. Impedance model of MMC has some specific properties in the high-frequency range: 1) most control effect diminish beyond near-synchronous frequency range [9], including phase-locked loop (PLL), dc voltage control and reactive power control; 2) sum capacitor voltage per MMC arm can be treated as constant above approximately $2f_1$. As a result, impedance model of MMC in high-frequency range can be interpreted as:

$$Z_p(s) = \frac{sL + G_d(s)\left[H_i(s - j\omega_1) - jk_d\right]}{1 + G_d(s)H_v(s)} = \frac{N_p(s)}{D_p(s)} \quad (1)$$

where $G_d(s) = e^{-s(T_{ds}/2+T_{di})}$ represents computation delay T_{di} and PWM delay $T_{ds}/2$. The ac current controller in dq-reference frame is modeled by $H_i(s - j\omega_1) - jk_d$, where k_d is the decoupling gain. H_v is the voltage controllers related to resonances above $2f_1$, such as grid voltage feed-forward control.

The overhead line $Z_g(s)$ is all the way passive but has a relatively small degree of passivity in a wide frequency range due to the small amount of inherent line resistance, while the GFL-MMC $Z_p(s)$ encounters a passivity shortage in the high-frequency range due to time delay generated phase lag [2]. Stability of the system shown in Fig. 1 is guaranteed if either both MMC and gird impedance is passive, indicating $\mathfrak{Re}\left[Z_p(s)\right] > 0$ and $\mathfrak{Re}\left[Z_g(s)\right] > 0$ (strictly stable condition) [9], or the net impedance is passive, indicating $\mathfrak{Re}\left[Z_p(s) + Z_g(s)\right] > 0$ (inclusively stable condition) [1].

B. Voltage-Based Damping Control Effect

Based on the above discussion, the MMC-grid resonance can be mitigated in such a way that the impedance of MMC around the resonance frequency is made to be passive (positive real). This can be achieved by incorporating additional damping control to reshape MMC impedance, and thus compensate the passivity at resonance frequency. To prevent unintended effects at other frequencies, the damping function with a filter

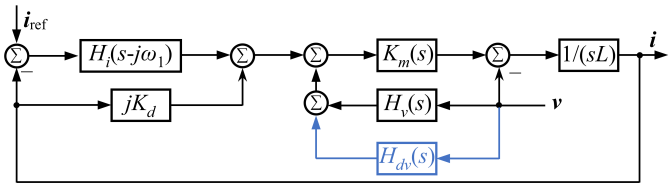

Fig. 2. Per-phase block diagram of the ac current control of GFL-MMC with voltage-based (blue) feed-forward control

is necessary to specify the frequency range of damping effect. In this vein, the narrowband damping function implemented in this work is based on a band-pass filter, which narrows the damping effect within a predetermined range. The per-phase block diagram of this damping scheme is shown in Fig. 2, in which $\boldsymbol{i}$ and $\boldsymbol{v}$ are the complex transfer functions of MMC output current i_{abc} and PCC voltage v_{abc} (as shown in Fig. 1). The grid voltage feed-forward loop with a low-pass sampling filter is represented by $H_v(s)$. $K_m(s)$ accounts for the modulation and switching process, introducing time delay described as $G_d(s)$. The damping controller $H_{dv}(s)$ uses ac voltage as its input and adds the output directly to the modulation signal of MMC, which is referred to as voltage-based narrowband damping scheme hereinafter. Since voltage-based damping introduces a term to the denominator of MMC impedance, the damping effect will be analyzed easily in terms of admittance. The admittance of GFL-MMC with such voltage-based damping scheme can be obtained as:

$$\begin{aligned} Y_{pdv}(s) &= \frac{1+G_d(s)\left[H_{dv}(s)+H_v(s)\right]}{sL+G_d(s)\left[H_i(s-j\omega_1)-jk_d\right]} \\ &= Y_p(s)+\frac{G_d(s)H_{dv}(s)}{N_p(s)} \end{aligned} \tag{2}$$

with the subscript *pdv* meaning the damped MMC admittance by voltage-based damping control. The voltage-based damping function can be viewed as introducing a virtual admittance in parallel with undamped MMC. It thus turns out that if the virtual impedance or admittance can be designed to be positive real around the resonance frequencies, the passivity of GFL-MMC can be enhanced and the resonances can be damped.

III. Narrowband Damping for Passivity Compensation

A. Multiple-Complex Coefficient-Filter

The first-order complex coefficient filter (CCF) synthesized in the discrete-domain as [10] is adopted here, and its multiple-paralleled expression can be written as:

$$H_{mccf}(z)=\sum_{k=1}^{n}\frac{(1-e^{-\omega_{bk}T_s})z}{z-e^{-(\omega_{bk}T_s-j\omega_{rk})T_s}} \tag{3}$$

The key parameters in (3) are as follows: ω_{rk} is the detected system resonance frequency which is also the filter center frequency, ω_{bk} is the bandwidth of the filter pass-band, T_s is the filter sampling period. The CCF has a settling time as $\tau_{bk}=5/\omega_{bk}$. It is worth noting that the sliding DFT (SDFT) filter used in [2], [11] and [12] is not fit for adaptive damping of HFR since its unacceptable long settling time. As an example, centering a CCF with 80 Hz bandwidth to an inter-harmonic frequency, such as 1023 Hz, takes 0.06 seconds; while to center an SDFT filter with the same bandwidth, it takes 1 second.

The purpose of narrowband damping is to add virtual positive conductance at the resonance frequency f_r, thus it is critical to compensate all kinds of phase lag posed upon band-pass filter. As can be seen from (2), the time delay, plant of current control and current control loop introduces phase lag to the added virtual admittance. The most straightforward phase lag compensation scheme is using phase-lead function $e^{j\theta}$, and θ is selected to be $-\angle G_d(j2\pi f_r)/N_p(j2\pi f_r)$.

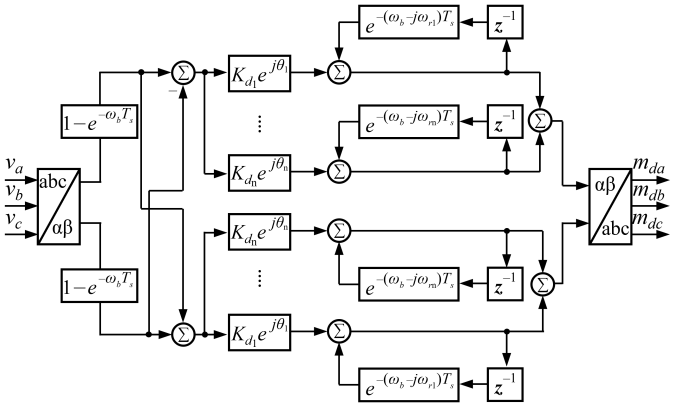

Fig. 3. Multiple-complex coefficient-filter based narrowband damping control structure

The conventional implementation of complex filter [13] in $\alpha\beta$-reference frame is adopted for the realization of multiple CCF (MCCF), where the cross-coupling terms are fully utilized. Fig. 3 shows the implementation of MCCF based damping control, where v_a, v_b and v_c are the input of three-phase voltage measurement and the output signals m_{da}, m_{db} and m_{dc} are directly added to MMC modulator input. The damping gain K_d is designed based on the desired amount of virtual conductance.

B. Design of Damping Function

1) Single-Tuned Damping Design

To iterate, the main goal of voltage-based narrowband damping is to emulate a virtual admittance with all positive real part around the resonance frequency f_r, in doing so, the non-passive region of MMC around f_r can be eliminated. To avoid resonance frequency drifting out of the damping band determined by the bandwidth of CCF, the magnitude of MMC admittance at f_r should be kept as constant as possible before and after damping. Therefore, the virtual admittance $K_dY_d(s)$ is programmed to achieve

$$K_d=\frac{2\left|\Re\mathfrak{e}\left\{Y_p(j2\pi f_r)\right\}\right|}{Y_d(j2\pi f_r)},\quad Y_d(s)=e^{j\theta}\frac{G_d(s)H_{ccf}(s)}{N_p(s)} \tag{4}$$

where K_d is damping gain given in pu based on the unit virtual admittance of $Y_d(s)$ at f_r. Note that, $H_{dv}(s)$ equals to $e^{j\theta}H_{ccf}(s)$.

2) Multi-Tuned Damping Design

MCCF can be employed to damp multiple resonances simultaneously. Each one is programmed to emulate a parallel admittance for the passivity compensation around a single resonance frequency. In such condition, the design should also consider the coupling effect among different programmed virtual admittance. Assume the multiple detected resonance frequencies are $f_{r1}, f_{r2}, ..., f_{rn}$, the damping gain for the

virtual admittance programmed at f_{rk} can be expressed by

$$K_{dk} = \frac{2\left|\mathfrak{Re}\left\{Y_p(j2\pi f_{rk})\right\}\right|}{Y_{dk}(j2\pi f_{rk})} + \frac{\left|\sum_{j=1,,j\neq k}^{n} \mathfrak{Re}\left\{Y_{dj}(j2\pi f_{rj})\right\}\right|}{Y_{dk}(j2\pi f_{rk})} \tag{5}$$

where the second term in (5) is to account for coupling effect between different damping functions. The damping gain vector $\boldsymbol{K}_d = [K_{d1}, K_{d2}, ..., K_{dn}]^{\mathrm{T}}$ can then be calculated by solving:

$$\boldsymbol{K}_d = \begin{bmatrix} \mathfrak{Re}\left\{\mathbf{Y}_{dk}(j\omega_{r1})\right\} \\ \mathfrak{Re}\left\{\mathbf{Y}_{dk}(j\omega_{r2})\right\} \\ \vdots \\ \mathfrak{Re}\left\{\mathbf{Y}_{dk}(j\omega_{rn})\right\} \end{bmatrix}^{-1} \cdot \mathrm{diag}(x_k) \cdot \begin{bmatrix} \mathfrak{Re}\left\{Y_p(j\omega_{r1})\right\} \\ \mathfrak{Re}\left\{Y_p(j\omega_{r2})\right\} \\ \vdots \\ \mathfrak{Re}\left\{Y_p(j\omega_{rn})\right\} \end{bmatrix} \tag{6}$$

where, $k = 1, 2, ..., n$ and $\omega_{rk} = 2\pi f_{rk}$. $\mathbf{Y}_{dk}(j\omega_{rk})$ are essentially row vectors with n entries, which represents the amount of conductance at f_{rk} provided by each unit virtual admittance at f_{rk}. Each element in $\mathbf{Y}_{dk}$ has the same form as $Y_d(s)$ in (5). Note that, in general, the entry in diag(x_k) can be specified based on damping design requirement, such as system stability margin requirement. However, when design the virtual admittance adaptively based on online resonance detection, the x_k is purposely programmed as 2 as the starting point of adjustment of x_k. Further adjustment of x_k should be based on the continuous evaluation of the MMC current behavior after conduction of damping control, which will be discussed in Section IV.

IV. Resonance Detection and Adaptive Passivity Compensation

A. Frequency Estimation of Spectral-Peak Related to Resonances

Spectral-peaks are prominent or dominant components in a spectrum and are sometimes referred to as maximum-amplitude components [14]. In a system with multiple simultaneous resonances, the amplitude spectrum is usually dominated by the resonance with the smallest net resistance [2], and one non-dominant resonance will immediately emerge and becomes the new dominant once the previously dominant one is mitigated. Traditional online resonance detection identifies a single resonance by simply picking the maximum-amplitude component from the spectrum, then comparing it with a predefined threshold value [7], [8]. Such a way cannot be directly applied to extract multiple resonance components from the spectrum, since cross-spectral interference between resonance components will introduce errors in frequency estimation.

However, the amplitude difference between the dominant and non-dominant resonances is usually significant, thus the cross-spectral interference can be considered as ignorable when estimating the dominant tone. In this work, the application of i-IpDFT [6] is extended to ensure an accurate estimation of the frequency of the multiple spectral-peaks related to resonances. The pseudocode of the proposed estimation algorithm is shown in Algorithm 1, where the idea behind is to iteratively eliminate the cross-spectral interference effect from estimated dominant resonance to non-dominant ones via subtracting its DFT image from the spectrum.

Algorithm 1 Frequency Estimation of Multiple Spectral-Peaks

1: $X_w(k) = \mathrm{DFT}[x_w(n)] - X_0^{\pm}(k)$
2: $k'_m = \mathbf{argmax}[X_w(k)]$;
3: $[f_m, A_m, \varphi_m, X_{f_m}^{\pm}(k)] = \mathrm{IpDFT}[X_w(k)]$ (from (7))
4: $X_w^R(k) = X_w(k) - X_{f_m}^{\pm}(k)$
5: Repeat line 2 to 4 based on reduced spectrum $X_w^R(k)$

As shown in Algorithm 1, the first step is to get the DFT spectrum of Hanning-windowed current measurement $x_w(n)$ and subtract the image of fundamental component from the spectrum to get $X_w(k)$, thus the spectral interference from fundamental component is totally eliminated (line 1). Next, IpDFT is applied to the $X_w(k)$ to obtain the frequency of the dominant resonance component, as well as its positive and negative image $X_{f_m}^{\pm}(k)$ (line 2, 3). Then, $X_{f_m}^{\pm}(k)$ is subtracted from $X_w(k)$, and IpDFT is applied to the resulting spectrum, of which the spectral interference from dominant resonance is eliminated (line 4). The process is then iterated until all the originally non-dominant resonances are estimated (lines 2 to 4). The equation for the IpDFT is given by

$$\begin{cases} \delta_m = 2\frac{\left|X_w(k'_m+1)\right| - \left|X_w(k_m-1)\right|}{\left|X_w(k'_m+1)\right| + 2\left|X_w(k'_m)\right| + \left|X_w(k'_m-1)\right|} \\ f_m = (k'_m + \delta_m)\Delta f; \quad \varphi_m = \angle X_w(k'_m) - \pi\delta_m \\ A_m = \left|X_w(k'_m)\right| \left|\frac{\pi\delta_m}{\sin(\pi\delta_m)}\right| \left|\delta_m^2 - 1\right| \\ X_{f_m}^{\pm}(k) = A_m e^{\pm j\varphi_m} W(k \mp f_m/\Delta f) \end{cases} \tag{7}$$

Being: δ_m the displacement bin frequency; f_m, A_m, φ_m the fine frequency, amplitude and phase angle of the highest DFT bin above 2^{nd} harmonic frequency; $W(k)$ the adopted Hanning-window function; $X_{f_m}^{\pm}(k)$ the positive and negative image of component with index k_m of the DFT bin.

B. Identification of Resonance

Fig. 4 depicts the overall process of online resonance detection based active damping. The MMC current is split by a fixed-length sampling window into a sequence of q short recording segments, and Hanning-windowed i-IpFFT is used to measure the short-time spectrum of each segment. To avoid spectral leakage of fundamental frequency component, the window length is selected to be one fundamental cycle ($1/f_1$). Next, the short-time spectrum in three-phase domain is further transformed into the positive and the negative sequence, where the largest amplitude $A^0(f_m^0)$ in the spectrum is then compared with a pre-settled threshold value A_{th} (normally 1% to 5% of the MMC rated current at fundamental frequency). f_m^0 is the frequency of spectral-peak or maximum-amplitude component. The subscript 'm' represents the maximum-amplitude component, while the superscript '0' indicates the spectrum is from a newly updated spectrum, in other words, a spectral analysis result based on the most updated time frame data. However, electrical transient can also be the spectral peak and exceed A_{th} in a short time period. To further characterize the maximum-amplitude component and identify the real

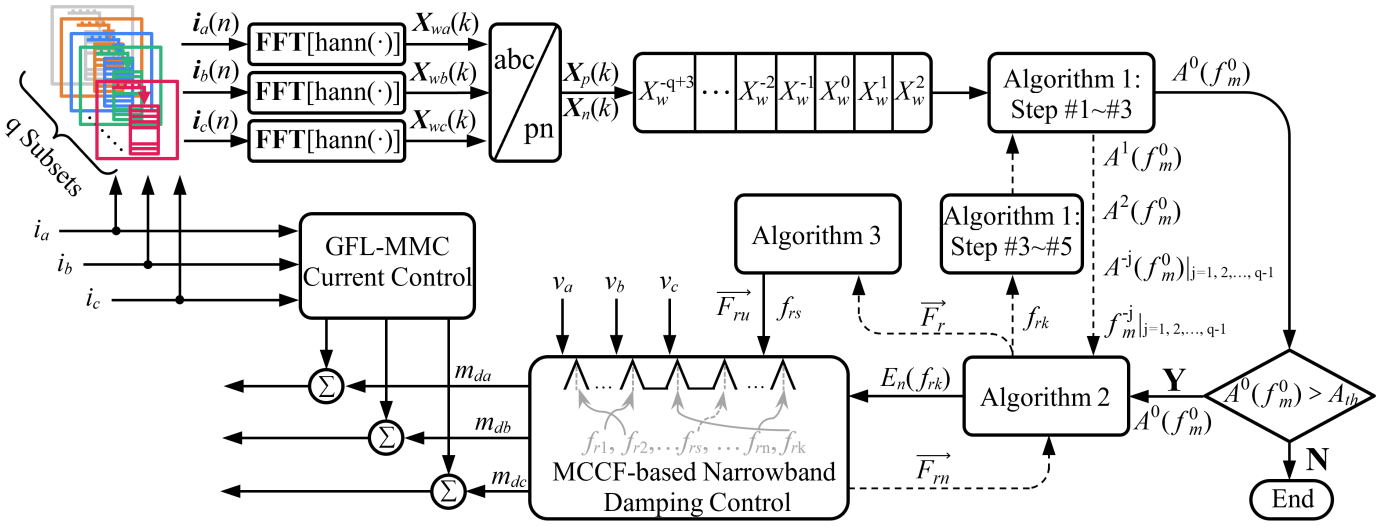

Fig. 4. Flowchart of proposed adaptive damping control based on online resonance detection

resonance from existing electrical transient, the Algorithm 2 is proposed in this section, which can be divided into the following two parts.

1) Distinguish Transient from Resonance (Line 1)

Considering the majority of transient signals below 5 kHz disappear within 50 ms [15], a simple identification method is to continuously monitor how the maximum-magnitude frequency bin in the most updated spectrum behaves in the next few time segments. In the condition that this component amplitude gradually decays, even to below A_{th} already in some cases, the MMC-grid system just needs to endure it until it disappears. For example, after getting $A^0(f_m^0)$ at frequency f_m^0, we extract component amplitudes at f_m^0 in the next two fundamental cycles first, which is denoted as $A^1(f_m^0)$ and $A^2(f_m^0)$. The component will be deemed as transient signal and the active damping control will not be conducted, if $A^2(f_m^0) < A^1(f_m^0) < A^0(f_m^0)$. Note that, $A^1(f_m^0)$ and $A^2(f_m^0)$ may not be the spectral peaks.

To fulfil the requirement on fast detection, N_{hop} samples are updated between each consecutive segments to regulate the detection speed. It is noteworthy that while smaller hop size N_{hop} will provide smoother spectral analysis results across time, they may lead to incorrect identification of resonance. A conservative constraint is to require that the total amount of recording time being used to monitor the behavior of maximum-amplitude component greater than 50 ms. That is, $(3N - 2N_{hop})/f_s > 50$ ms, where f_s is the sampling frequency and N is the number of samples per window.

2) Determination of Resonance (Line 2~7)

After knowing the spectral peak at f_m^0 is not from a transient oscillation, the second part start with checking if the maximum-amplitude components in the past (q-1) windows are all at f_m^0 (line 2~4). In the case that all the spectral peaks in the (q-1) windows are at f_m^0, the proposed algorithm will further check whether these maximum-amplitudes are all larger than A_{th} (line 6). If so, f_m^0 is stored into a vector $\overrightarrow{F_{rn}}$ with all early detected resonance frequencies and an enabling signal $E_n(f_{rk})$ is also sent to the next block to center a CCF based damping controller to f_{rk} (line 7~8).

Algorithm 2 Identification of the Resonance

Input: 1) f_m^0; 2) $A^0(f_m^0)$, $A^1(f_m^0)$ and $A^2(f_m^0)$; 3)$\overrightarrow{F_{rn}} = (f_{r1}, f_{r2}, ..., f_{rn})$;
Output: 1) $\overrightarrow{F_r} = (f_{r1}, f_{r2}, ..., f_{rn}, f_{rk})$; 2) $E_n(f_{rk})$

1: **if** $A^2(f_m^0) < A^1(f_m^0) < A^0(f_m^0)$ **then** $\overrightarrow{F_r}$=$\overrightarrow{F_{rn}}$; $E_n(f_{rk})$=0;
2: **else**
3: **for** $j = 1, 2, 3, \ldots, q-1$ **do**
4: **if** $A^{-j}(f_m^0) < A_{th}$ **then** $\overrightarrow{F_r}$=$\overrightarrow{F_{rn}}$; $E_n(f_{rk})$= 0;
5: **else**
6: **if** $f_m^{-(q-1)} = f_m^{-(q-2)} = ... = f_m^{-1} = f_m^0$ **then**
7: $k = \textbf{sizeof}(\overrightarrow{F_{rn}})+1$, $\overrightarrow{F_r}(k) = f_m^0$, $f_{rk} = f_m^0$,
8: $E_n(f_{rk}) = 1$

C. Remove Redundant Damping Controls

In a practical system, an unstable resonance could quickly be cleared as the changed passive grid can provide sufficient damping at that frequency. In this subsection, we propose the Algorithm 3, capable of automatically disconnecting previously employed damping controllers one by one, but if a resonance is still present, the algorithm turn on the corresponding damping control again.

The method starts in line 1, with the assignment of all the previously detected resonance frequencies to $\overrightarrow{F_{ru}}$. A sorting process is then performed to determine the resonance frequency f_{rs} at which the MMC has the smallest negative damping (line 2). Since the algorithm assumes the new resonance is a result of grid variation, and some previously detected resonance may already have disappeared, it disables the damping controller centering to f_{rs} first (line 3~5). In addition, MCCF based multi-tuned damping will be re-programmed and only tackle to the remaining resonance frequencies (line 6). The design of MCCF based multi-tuned damping will take the resonance at f_{rs} into account again if a new resonance

Algorithm 3 Remove Redundant Damping Controls

Input: $\overrightarrow{F_r}$= $(f_{r1}, f_{r2}, ..., f_{rn}, f_{rk})$;
Output: 1) $\overrightarrow{F_{ru}}$; 2) f_{rs}
1: $\overrightarrow{F_{ru}} = (f_{r1}, f_{r2}, ..., f_{rs}, ..., f_{r(n-1)}, f_{rn}, \cancel{f_{rk}})$;
2: **for** $s = 1, 2, 3, \ldots,$ **sizeof**$(\overrightarrow{F_r})$ **do**
3: Take the frequency f_{rs} at which the MMC has the lowest negative damping among all the $\Re\mathfrak{e}\,[Z_p(j2\pi f_r)]$, $f_r \in \overrightarrow{F_r}$
4: $\overrightarrow{F_{ru}}$= $(f_{r1}, f_{r2}, \ldots, \cancel{f_{rs}}, \ldots, f_{r(n-1)}, f_{rn})$
5: $\overrightarrow{F_r}$=$(f_{r1}, f_{r2}, \ldots, \cancel{f_{rs}}, \ldots, f_{r(n-1)}, f_{rn})$
6: Program MCCF based on $\overrightarrow{F_{ru}}$
7: **if** newly detected resonance frequency $f_{new} < f_{rs} \pm \omega_b/(2\pi)$ **then**
8: Include f_{rs} in $\overrightarrow{F_{ru}}$; Program MCCF based on $\overrightarrow{F_{ru}}$; Repeat from line 2
9: **else**
10: Repeat from line 2

around f_{rs} reappears (line 7∼8). Otherwise, it indicates that the damping control is not required around f_{rs}. Multiple iterations of the above procedures may be conducted until all the disappeared resonances are identified, and corresponding damping controls are turned off (line 9∼10).

V. Case Study and Simulation Validation

To validate the performance of the proposed adaptive damping method for MMC passivity compensation, two application exmaples based on detailed EMT simulations are presented in this section. The key parameters are as follows:

- GFL-MMC: Arm inductor = 50 mH; PLL bandwidth = 15 Hz; current control loop bandwidth = 200 Hz; The phase margin of each loop is 45°; Time delay = 200 μs; Rated AC output voltage = 300 kV at 50 Hz; CCF bandwidth in radians ω_b = $2\pi 80$.
- Online detection: Sampling frequency f_s = 100 kHz; N = 2000, N_{hop} = 1000; q = 3; A_{th} = $5\%I_g$, where I_g is the amplitude of rate at fundamental frequency.

A. Damping of Multiple HFRs between GFL-MMC and OTL

The first example involves a GFL-MMC connected to a 150-km overhead transmission line (OTL) through a 300/345 kV step-up transformer, where HFR appears at two frequencies simultaneously.

As can be seen from Fig. 5 c), when GFL-MMC start connecting to OTL, an electrical transient is initiated at 716 Hz and it dominates the short-time spectrum of two consecutive time recording segments. This tranisent is correctly identified by the Algorithm 2, thereby no active damping control reacts to it. An unstable 1539 Hz resonance is measured at t = 0.082 s, where the single-tuned damping control is conducted, which adds positive resistance around 1539 Hz. By using (4), the parameters of the single-tuned damping control are automaticlly calculated as: f_{r1} = 1539 Hz, K_{d1} = 0.1594, θ_1 = -154.81°. Following this event, another unstable resonance at 2390 Hz begins to grow, which is detected at t = 0.328 s. A double-tuned damping control is then programmed to add

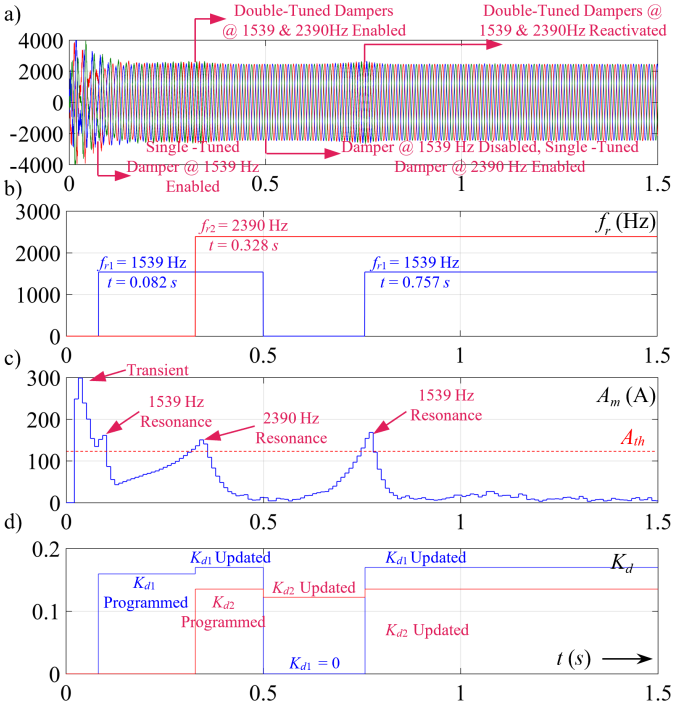

Fig. 5. a) Simulated time-domain responses of MMC current. Online processing data: b) detected resonance frequency f_r; c) The maximum-amplitude component in FFT spectrum; d) damping gain of CCFs

positive resistance at both resonance frequency. Based upon (6), the parameters of the double-tuned damping control are given by: f_{r1} = 1539 Hz, K_{d1} = 0.1697, θ_1 = -154.81°; f_{r2} = 2390 Hz, K_{d2} = 0.1352, θ_2 = -94.71°.

At t = 0.5 s, the Algorithm 3 starts to disable the damping control at 1539 Hz, and the double-tuned damping control adjusts to single-tuned damping centering to 2390 Hz only. It should be noted that the damping control parameters have to be updated in order to ensure that the added positive resistance at 2390 Hz remains constant unchanged. Because otherwise, the 2390 Hz may not be well mitigated. The parameters single-tuned damping are updated to: K_{d1} = 0, f_{r2} = 2390 Hz, K_{d2} = 0.1222, θ_2 = -94.71°. From Fig. 5, it can be seen that the 1539 Hz resonance starts again after damping control at 1539 Hz is disabled, indicating a need for prgramming damping control at both 1539 Hz and 2390 Hz. The double-tuned damping control is automatically reactivated at t = 0.757 s, and the 1539 Hz resonance is suppressed.

The impedance of undamped MMC (Z_p), the impendace of damped MMC with the above-mentined double-tuned damping control (Z_{p2d}) and single-tuned damping control at 2390 Hz (Z_{pd}) are plotted against OTL impedance (Z_g). The undamped MMC and OTL form two series resonance at 1539 Hz and 2390 Hz, where the net resistance at 1539 Hz is $\Re\mathfrak{e}\,[Z_p(j2\pi 1539) + Z_g(j2\pi 1539)]$ = -9.43 Ω, while the net resistance at 2390 Hz is $\Re\mathfrak{e}\,[Z_p(j2\pi 2390) + Z_g(j2\pi 2390)]$ = -3.11 Ω, indicating double unstable HFRs. With the added double-tuned damping control, the net-resistance ($\Re\mathfrak{e}\,[Z_{p2d}(j2\pi f_r) + Z_g(j2\pi f_r)]$) at the two intersection frequencies are compensated to 25.47 Ω and 38.97 Ω, indicating that the system is strictly-stable. With only single-

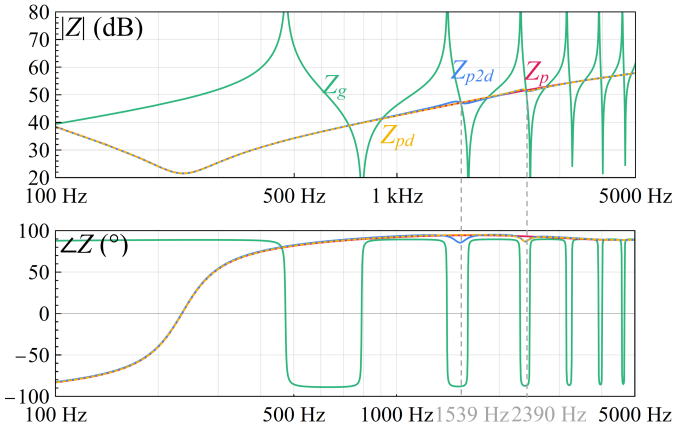

Fig. 6. Impedance responses of: undamped GFL-MMC (red), damped MMC with double-tuned damping control (blue), damped MMC with single-tuned damping control (orange) against OTL impedance (green)

tuned damping control applied at 2390 Hz, the net-resistance ($\Re\mathfrak{e}\,[Z_{pd}(j2\pi f_r) + Z_g(j2\pi f_r)]$) at 2390 Hz changes to 39.32 Ω, which remains almost the same as before. However, net-resistance at 1539 Hz decreases to -11.68 Ω, signifying an unstable resonance as shown in MMC current response between 0.5 *s* and 0.757 *s*. The passivity-based stability analysis further confirms the effectiveness of the proposed adaptive damping control.

B. Damping HFR Changed with Grid Variation

The aim of this subsection is to test the robustness of the proposed adaptive damping control against grid variation. However, the example also represents a practical reason of HFR in MMC based HVDC systems [16]. The schematic of the simulation model used to test the adaptive control is depicted in Fig. 7. The simulation starts with MMC connnects to the ac system through Line 1, in which Line 2 and Line 3 are initially disconnected from the ac system. At t = 0.2 *s*, the grid 2 is connected to the ac system via Line 2. At t = 0.5 *s*, the Line 2 is cut off and grid 3 is connected the ac system via Line 3. The simulated GFL-MMC current response and the data used for online detection are shown in Fig. 8. The first resonance is measured to be 2293 Hz at t = 0.246 *s* after Line 2 is connected, then a single-tuned damping control at 2293 Hz is conducted. By using (4), the parameters of the single-tuned damping control are automaticlly calculated as: f_{r1} = 2293 Hz, K_{d1} = 0.1317, θ_1 = -101.47°. Following cutting off Line 2 and the connection of Line 3, the second resonance is measured to be 2606 Hz at t = 0.563 *s*. Based on the adaptive damping control proposed in this work, a double-tuned damping control is designed first

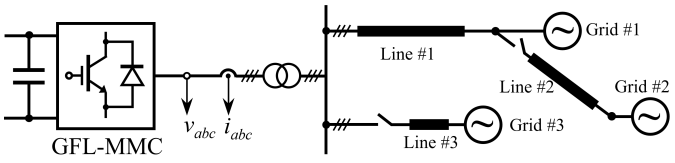

Fig. 7. Schematic of the GFL-MMC against ac grid in second example

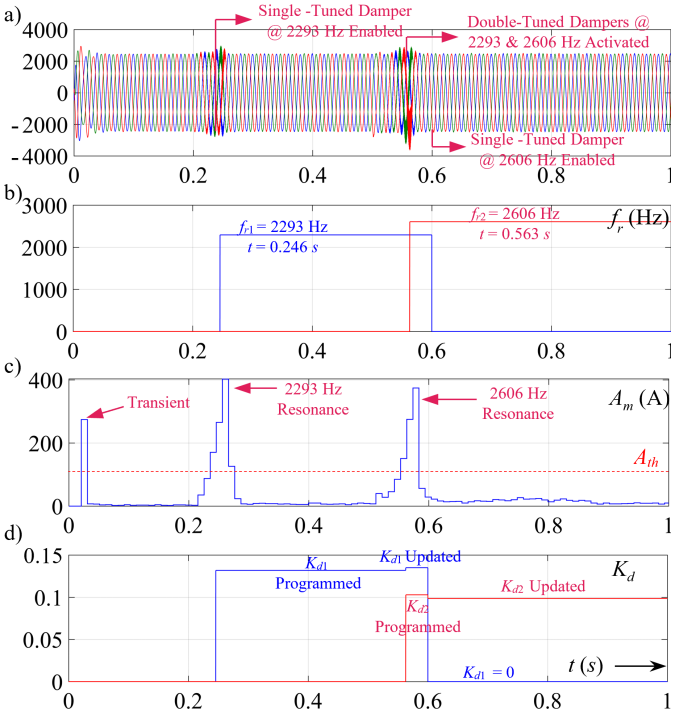

Fig. 8. a) Simulated time-domain responses of MMC current. Online processing data: b) detected resonance frequency f_r; c) The maximum-amplitude component in FFT spectrum; d) damping gain of CCFs

to compensate the passivity of MMC at both 2293 Hz and 2606 Hz, which immediately damped the resonance at 2606 Hz resonance. The parameters of the double-tuned damping control are given by: f_{r1} = 2293 Hz, K_{d1} = 0.135, θ_1 = -101.47°; f_{r2} = 2606 Hz, K_{d2} = 0.103, θ_2 = -79.87°. To test whether the new resonance is a result of grid variation, the Algorithm 3 disables the damping control at 2293 Hz at t = 0.6 *s*, and the double-tuned damping control is adjusted to a single-tuned damping centered at 2606 Hz only. The parameters of single-tuned damping are updated to: K_{d1} = 0, f_{r2} = 2606 Hz, K_{d2} = 0.0986, θ_2 = -94.71°. As can be seen from Fig. 8, without damping control at 2293 Hz, the system shows a stable operation, indicating the 2293 Hz resonance disappears. Thus, the proposed online detection algorithm can identify the grid variation and the adaptive control can correspondingly eliminate redundant damping controls, signifying a high robustness to grid variation.

VI. Conclusion

This paper has introduced an adaptive narrowband damping control, which can suppress multiple HFRs with unknown frequencies. The i-IpDFT based spectral-peak detection algorithm and the resonance identification algorithm have been proposed and discussed, which provides an accurate estimation of multiple HFRs. As a result, the MMC is able to adaptively program multi-tuned narrowband damping control for mitigating HFRs during the integration into unknown systems. To ensure the robustness of adaptive damping control, an adaptive rule is proposed for identifying the disappeared resonances and disconnecting corresponding damping controls under varing gird

condition. Detailed EMT simulation validates the effectiveness of the proposed adaptive passivity compensation method.

REFERENCES

[1] L. Harnefors, "Proof and application of the positive-net-damping stability criterion," *IEEE Transactions on Power Systems*, vol. 26, pp. 481–482, February 2011.

[2] P. Huang and J. Sun, "Mitigation of MMC high-frequency resonance by narrowband damping," in *2021 IEEE 22nd Workshop on Control and Modelling of Power Electronics (COMPEL)*, pp. 1–7, IEEE, 2021.

[3] I. Vieto, P. Huang, and *et al.*, "Online measurement of offshore wind farm impedance for adaptive control of HVDC transmission systems," in *2019 20th Workshop on Control and Modeling for Power Electronics (COMPEL)*, pp. 1–8, IEEE, 2019.

[4] D. Agrež, "Weighted multipoint interpolated dft to improve amplitude estimation of multifrequency signal," *IEEE Transactions on Instrumentation and Measurement*, vol. 51, pp. 287–292, April 2002.

[5] P. Romano and M. Paolone, "Enhanced interpolated-DFT for synchrophasor estimation in FPGAs: Theory, implementation, and validation of a pmu prototype," *IEEE Transactions on Instrumentation and Measurement*, vol. 63, no. 12, pp. 2824–2836, 2014.

[6] A. Derviškadić, P. Romano, and M. Paolone, "Iterative-interpolated dft for synchrophasor estimation: A single algorithm for p- and m-class compliant pmus," *IEEE Transactions on Instrumentation and Measurement*, vol. 67, no. 3, pp. 547–558, 2018.

[7] W. Cao, Y. Ma, and F. Wang, "Adaptive impedance compensation of inverters for stable grid integration based on online resonance detection," in *2019 IEEE Applied Power Electronics Conference and Exposition (APEC)*, pp. 3151–3158, IEEE, 2019.

[8] J. Man, L. Chen, V. Terzija, and X. Xie, "Mitigating high-frequency resonance in mmc-hvdc systems using adaptive notch filters," *IEEE Transactions on Power Systems*, pp. 1–1, 2021.

[9] L. Harnefors, X. Wang, A. G. Yepes, and F. Blaabjerg, "Passivity-based stability assessment of grid-connected VSCs—An overview," *IEEE Journal of Emerging and Selected Topics in Power Electronics*, vol. 4, pp. 116–125, March 2016.

[10] E. Guest and N. Mijatovic, "Discrete-time complex bandpass filters for three-phase converter systems," *IEEE Transactions on Industrial Electronics*, vol. 66, no. 6, pp. 4650–4660, 2019.

[11] H. Bai, X. Wang, and F. Blaabjerg, "A grid-voltage-sensorless resistive-active power filter with series LC-filter," *IEEE Transactions on Power Electronics*, vol. 33, pp. 4429–4440, May 2018.

[12] J. He, Y. Li, and M. S. Munir, "A flexible harmonic control approach through voltage-controlled DG–grid interfacing converters," *IEEE Transactions on Industrial Electronics*, vol. 59, pp. 444–455, January 2012.

[13] X. Guo, W. Wu, and Z. Chen, "Multiple-complex coefficient-filter-based phase-locked loop and synchronization technique for three-phase grid-interfaced converters in distributed utility networks," *IEEE Transactions on Industrial Electronics*, vol. 58, pp. 1194–1204, April 2011.

[14] J. O. Smith, *Spectral Audio Signal Processing*. New York, NY, USA: W3K, 4th ed., 2011.

[15] "IEEE recommended practice for monitoring electric power quality,," *IEEE Std 1159-2019 (Revision of IEEE Std 1159-2009)*, pp. 1–98, 2019.

[16] C. Zou and *et al.*, "Analysis of resonance between a VSC-HVDC converter and the ac grid," *IEEE Transactions on Power Electronics*, vol. 33, pp. 10157–10168, February 2018.